ICFA
17TH ADVANCED BEAM DYNAMICS WORKSHOP ON
FUTURE LIGHT SOURCES

Aspects of Strong-Focusing Undulator Design for Storage Ring and Linac-Driven X-ray FEL (XRFEL) Applications

R. Tatchyn, SSRL/SLAC

APRIL 6-9, 1999
ARGONNE NATIONAL LABORATORY, ARGONNE, IL U.S.A.

Aspects of strong-focusing undulator design for storage ring and linac-driven X-ray FEL (XRFEL) Applications*

Roman Tatchyn[a]

Stanford Synchrotron Radiation Laboratory, Stanford Linear Accelerator Center, Stanford, CA 94305, USA

Talk Outline

- strong-focusing insertion device applications
    - storage rings
    - linacs (FELs)
- selected strong-focusing techniques
- planar permanent magnet multipoles
- strong-focusing insertion device designs
- summary

*This work was supported in part by the Department of Energy Offices of Basic Energy Sciences and High Energy and Nuclear Physics, and Department of Energy Contract DE–AC03–76SF00515.
[a]Corresponding author: Email: tatchyn@ssrl01.slac.stanford.edu; TEL: 650-926-2731; FAX: 650-926-4100

- **strong-focusing insertion device applications:**

  - storage rings: short-period insertion devices:

$$P = \frac{2}{3}\frac{e^2}{c}\gamma^6\left[\left(\dot{\boldsymbol{\beta}}\right)^2 - \left(\boldsymbol{\beta}\times\dot{\boldsymbol{\beta}}\right)^2\right] \quad (CGS)$$

For a sinusoidal trajectory,

$$P \cong \frac{2}{3}\frac{e^2}{c}\gamma^4\left(\dot{\boldsymbol{\beta}}_{\mathrm{perp}}\right)^2.$$

In terms of undulator parameters,

$$P = \frac{2e^2}{3c}\left(\frac{2\pi K c^2}{\gamma}\right)^2 = \frac{2e^2}{3c}\frac{\left(2\pi K c^2\right)^2}{\lambda}\frac{\left(1+\left(K^2/2\right)\right)}{2\lambda_u}$$

Effect on Brightness (assume fixed K, fixed λ, fixed undulator length):

- **reduce $\lambda_u \rightarrow \lambda'_u$ => reduce energy by** $\sqrt{\frac{\lambda'_u}{\lambda_u}}$
- **in-band flux $\propto N_u$ => Brightness** $\propto \frac{1}{\lambda_u{}^2}$

(but must also consider effect of energy reduction on the emittance)

- **reduced-period, smaller-gap undulators can[1,2,3,4]:**

    1) substantially increase brightness at a higher photon energy ($Brt \propto N_u$):
    2) reduce storage ring energy (by the square root of period reduction)
    3) for K > 1.4, increase in-band output flux with 1/(period reduction)

- **requirements:**

    1) high (0.5T-2T) fields for large gap/period ratios ($0.5 < g/\lambda_u < 1$):
    2) maximal length (up to the limit of available straight sections)

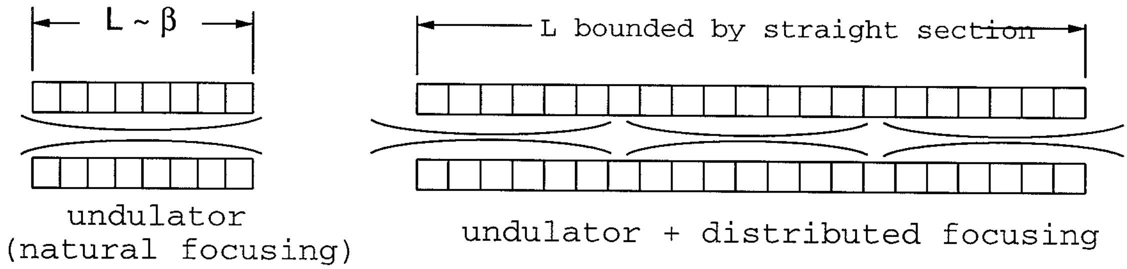

- **collateral storage ring requirements[5]:**

    - reduced COULOMB scattering => reduced vacuum

    - reduced beam scraping => reduced emittance

---

1. G. Brown, H. Winick, P. Eisenberger, Nucl. Instrum. Meth. 204, 543(1983).
2. P. Csonka, SPIE Proceedings 582, 298(1986).
3. R. Tatchyn, P. Csonka, A. Toor, Rev. Sci. Instrum. 60(7), 1797(1989).
4. P. M. Stefan and S. Krinsky, Rev. Sci. Instrum. 67(9), 1996.
5. R. Tatchyn, "PERSPECTIVES ON THE USE OF MICROPOLE IDs IN ULTRA-LOW EMITTANCE 4TH GENERATION STORAGE RINGS," in Proceedings of the 10th ICFA Beam Dynamics Panel Workshop on 4th Generation Light Sources, J.-L. Laclare, Ed., ESRF, Grenoble, 1/22-25/96, pp. WG-116 - WG-122..

- linacs (FELs):

FEL gain parameter

$$\rho = \gamma^{-1}\left(5.6\times 10^{-15} K^2 n_e \lambda_u{}^2\right)^{\frac{1}{3}}$$

Use $n_e = I_p / 2\pi c q \varepsilon\beta$, $\lambda_u = 2\gamma^2\lambda/\left(1+K^2\right)$, $\beta^{-2} = \beta_u{}^{-2} + \beta_{ext}{}^{-2}$.

For $\varepsilon = \lambda/2\pi$,

$$\rho = \gamma^{-1}\left(7.37\times 10^{-6}\gamma I_p \left(\frac{K^3}{1+K^2}\right)\left(1+\left(\frac{\beta_u}{\beta_{ext}}\right)^2\right)^{\frac{1}{2}}\right)^{\frac{1}{3}}.$$

Three regions of optimization are defined by whether $\beta_u \ll \beta_{ext}$, $\beta_u \approx \beta_{ext}$, or $\beta_u \gg \beta_{ext}$. For the last, or "weak-field" case, leading to an optimum K value of 1,

$$\rho = \left[\frac{1.17\times 10^{-6}\lambda I_p \gamma}{\beta_{ext}}\right]^{\frac{1}{3}}.$$

- **R&D at SSRL:**

1) high-field undulator designs with periods down to ~ 1mm[5,6,7]
2) operation of submillimeter period undulators on the LLNL linac[7]
3) PM quadrupole development for distributed focusing in small gaps[8,9,10,11]

---

5. A. Toor, P. Csonka, R. Tatchyn, Rev. Sci. Instrum. 60(7), 1439(1989).
6. A. S. Khlebnikov, N. S. Osmanov, A. V. Smirnov, and R. Tatchyn, "A STRONG FOCUSING UNDULATOR SCHEME," ibid., ms. Tu-3-54.
7. R. Tatchyn, A. Toor, J. Hunter, R. Hornady, D. Whelan, G. Westenskow, P. Csonka, T. Cremer, and E. Kallne, Journal of X-Ray Science and Technology 1, 79(1989).
8. R. Tatchyn, Nucl. Instrum. Meth. A341, 448(1994).
9. R. Tatchyn, IEEE Trans. Mag. 30(6), 5050(1994).
10. R. Tatchyn, T. Cremer, Proc. PAC '95 Conference.
11. R. Tatchyn, "A field-cancellation algorithm for constructing economical planar permanent magnet (PM) multipoles with large high-quality field apertures* Proceedings of the 1997 Particle Accelerator Conference, Vancouver, B. C., Ms. 9P121.

- **selected strong-focusing techniques**

- STI (wedged-pole): NISUS[12]

- Schlueter (wedged/canted pole)

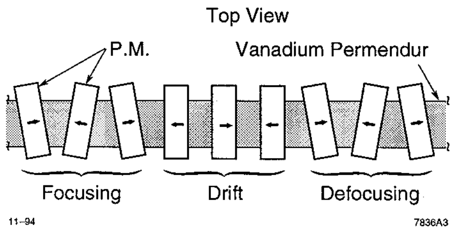

- planar permanent magnets (Tatchyn, Pfluger, Nikitina, Varfolomeev)

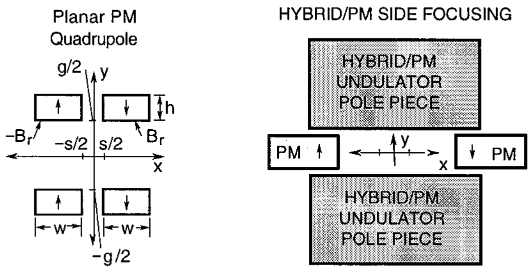

- for the planar permanent magnet quad FODO lattice

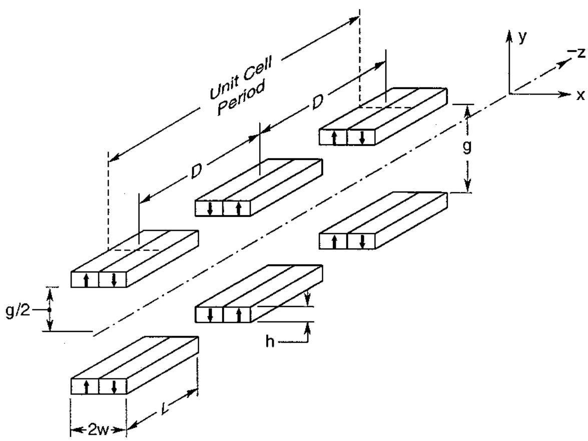

$$f \cong \frac{4E[GeV]\left(g^2 + 2gh\right)}{3B_r L h} \quad ,\cdot\ \beta_{ext}=2f.$$

12. D. C. Quimby, S. C. Gottschalk, F. E. James, K. E. Robinson, J. M. Slater, and A. S. Valla, "Development of a 10-meter wedged-pole undulator," Nucl. Instrum. Meth. A285, 281(1989).

- **planar permanent magnet multipoles**

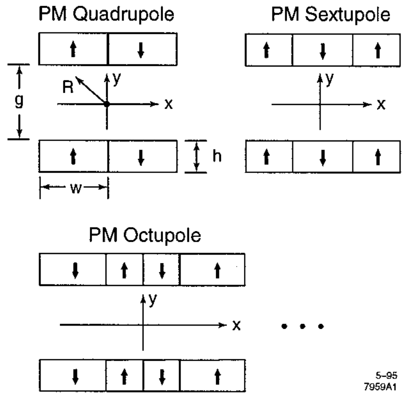

Figure 1. Planar PM multipoles composed of pieces of equal height (h), with no lateral spacing between pieces. Symmetry axis (z axis), along which all the PM pieces have equal length L, is perpendicular to the page.

Can partition planar PMMs into two classes:

$$\phi_{4n} \cong C_{11}xy + E_{13}(xy^3 - x^3y) + G_{15}(3xy^5 - 10x^3y^3 + 3x^5y) + \ldots$$

and

$$\phi_{4n-2} \cong B_{01}y + D_{21}(3x^2y - y^3) + F_{41}(5x^4y - 10x^2y^3 + y^5) + \ldots$$

Reduced symmetry =. poor field about axis

To improve field quality, use linear superposition

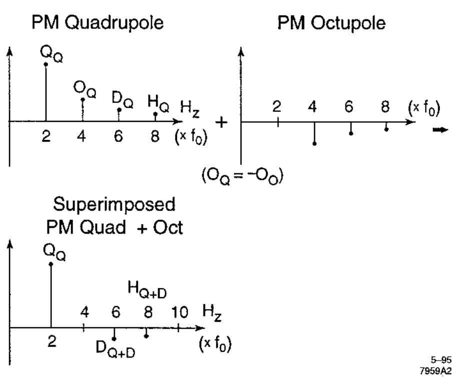

Figure 2. Linear superposition of planar PM octupole and quadrupole fileds as a means of nulling the octupole component in the combined structure.

- **basic field-improvement strategy:**

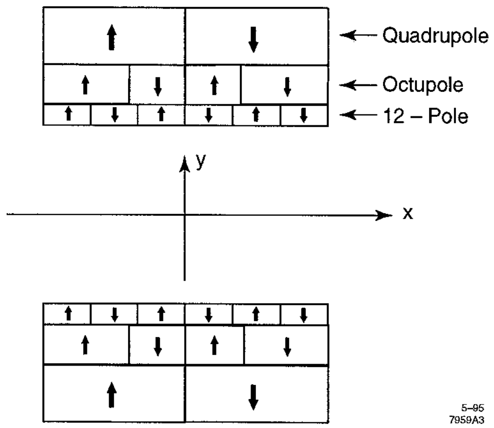

Figure 3. Planar PM quadrupole structure with nulled octupole and dodecapole field components.

- **improved field-improvement strategy:**

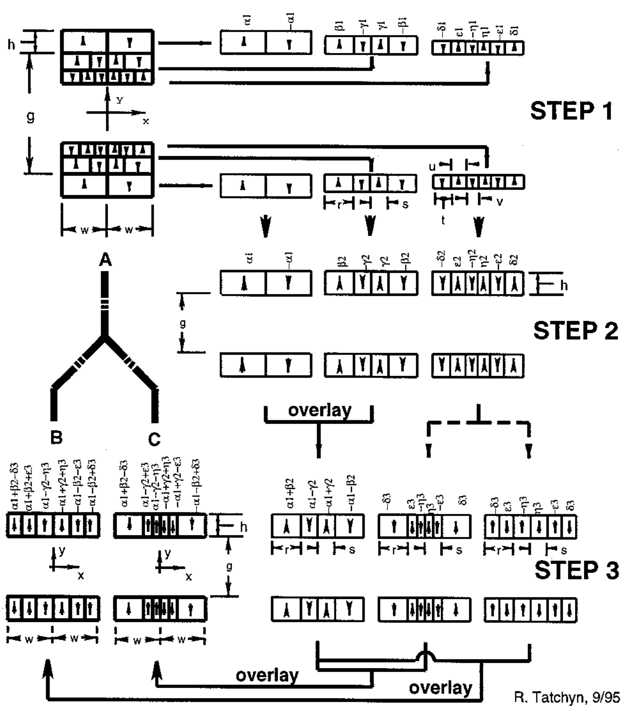

Figure 4. Planar PM quadrupole field-cancellation algorithm for removing octupole and dodecapole components with a minimal number of pieces. Structures B and C are, apart from a scalar factor, equivalent to A.

- **strong-focusing insertion device designs**

- Khlebnikov design:

Strong Focusing Undulator

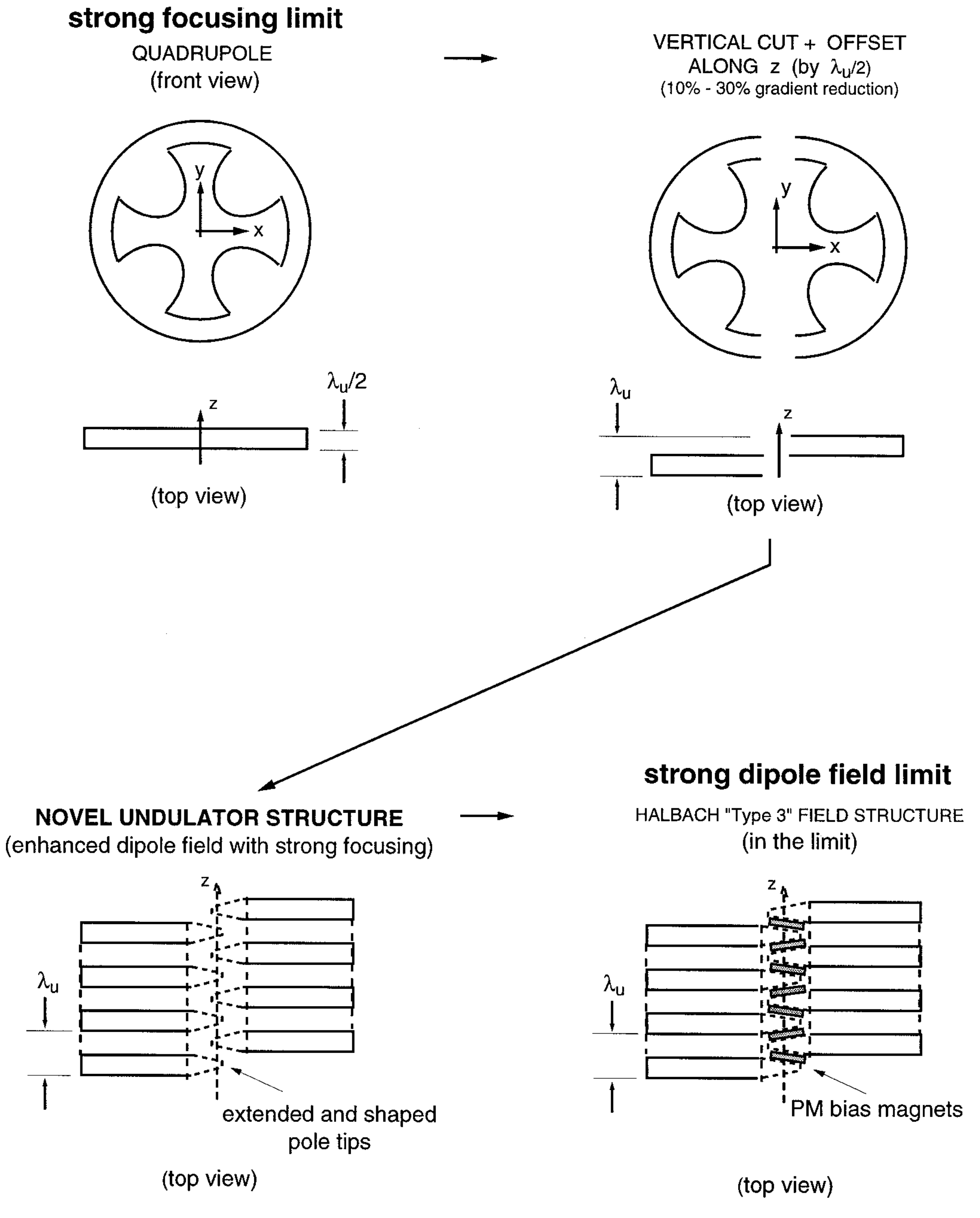

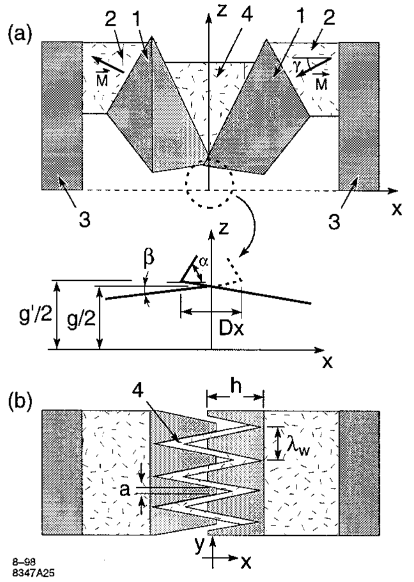

Figure 1. Improved undulator structure: a) - side view of the top part of the structure; b) - top view. 1 - steel yokes; 2 - PM material; 3 - steel plates; 4 - bias PM pieces (Case 2 only).

- low-emittance LCLS design:

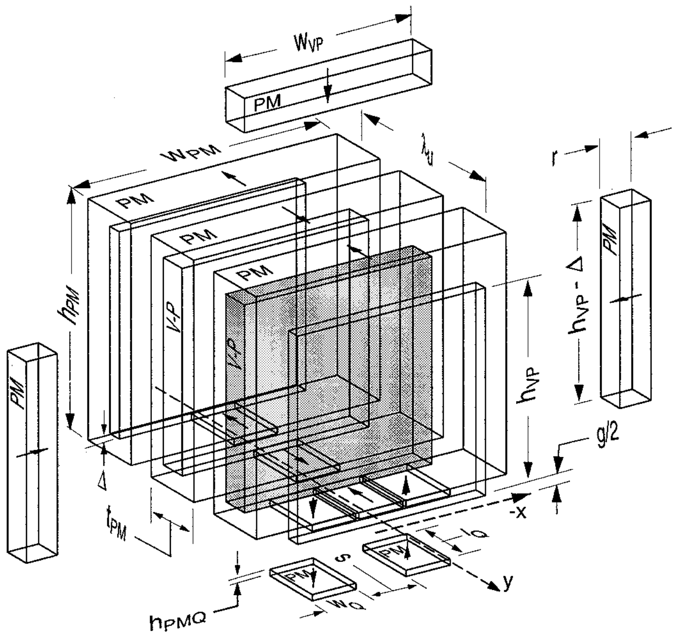

Figure 1. Undulator components and design options (structure mirror-symmetric with respect to the x-y plane; top half shown). To maximize or shim the on-axis field, each pole piece can have one top and two side bias pieces appended to it. Bevels on pole surface edges not shown. For the recessed PMQs, $l_Q = t_{PM}$ and $s = w_{smin}$.

- SLAC LCLS design[13]:

- segmented structure (52 1.92 meter segments)
- segment separation (0.235 meter)
- interleaved FODO lattice
- $< 10^{-7}$ Torr vacuum
- beam based alignment
- wakefield effects in vacuum duct

13. R. Carr et al, "The LCLS Undulator," presented at the 20th International FEL Conference (FEL98), August 16-21, Williamsburg, VA, 1998, ms. Tu-3-49.

14. Undulator

Undulator Properties

		Units
Overall length, including separations	111.825	m
Undulator magnet length	99.84	m
Start location after cathode	1161	m
Undulator type	planar hybrid undulator	
Magnet material	NdFeB	
	40 mm x 10 mm x 30 mm	
Permeable material	Va Permendur	
	36 mm x 5 mm x 25 mm	
undulator period λ_u	30	mm
Full gap g	6	mm
Undulator field B_{max}	1.32	T
Undulator parameter K	3.71	
a_u (K / 2)	2.62	
Number of periods per segment	64	
Number of segments	52	
Separation between segments	0.235	m
Segment magnet length	1.92	m
Number of periods N_u	3328	
Wiggle plane	vertical	

Electron Beam Optics

Focusing method	separated function	
Focusing scheme	FODO	
Quadrupole length	12	cm
Quadrupole type	permanet magnet	
Cell length	4.32	m
Quadrupole gradient	45.5	T/m

14. Undulator (continued)

			Units
Electron energy	4.54	14.35	GeV
Average β-function	6.1	18.0	m/rad
Maximum β-function (Initial β_x)	8.4	20.1	m/rad
Minimum β-function (Initial β_y)	3.8	15.9	m/rad
Beta-function modulation	76	23	%
Phase advance per cell	45	13	degrees

Electron Trajectory Correction

		Units			
Trajectory correction scheme	quadrupole displacement				
Center distance between steering quads	2.16	m			
Number of steering quads	52				
Maximum transverse quad displacement	500	μm			
(In horizontal and vertical plane)					
Maximum trajectory slope angle			180.3	57.0	μrad
Number of beam position correctors	52				
Number of carbon wire stations	10				

Electron Beam Parameters at Entrance

Electron energy		4.54	14.35	GeV	
Normalized emittance		2.00	1.50	π mm mrad	
Correlated energy spread		0.10	0.10	%	
Uncorrelated energy spread	.014	0.003	0.001	%	col
rms bunch length L_B		20	20	μm	
FWHM bunch length $L_{B,FWHM}$		233	233	fs	
Pulse charge		0.95	0.95	nC	
Peak current		3400	3400	A	
Longitudinal brightness		226	226	A	

Electron Beam Parameters inside the Undulator

Electron beam radius (rms)	37	31	μm
Electron beam divergence (rms)	6.1	1.7	μrad
Maximum undulation angle	418	132	μrad
Maximum pk-pk undulation amplitude	4.0	1.3	μm
Maximum disp. function for ideal undulator	4.0	1.3	μm

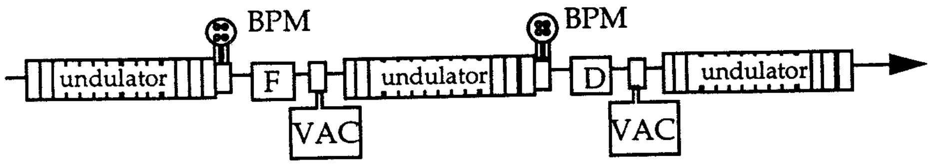

Figure 8.1-1. A schematic side view of the undulator structure, showing the FODO lattice with separations between 1.92 m undulator sections for diagnostics, focusing correctors, and vacuum ports. The undulator magnets are mounted on aluminum girders whose temperature is stabilized.

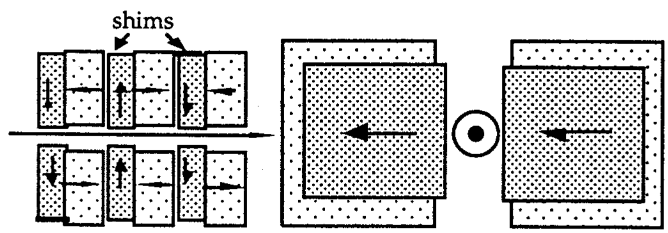

Figure 8.1-3. Left: Top view of undulator, showing shims on poles and small gaps between pole assemblies. Shims may also be applied to the gapside faces of the NdFeB. Right: End view of undulator, showing NdFeB overlapping vanadium permendur pole pieces. The field of the undulator is horizontal, so that the radiation is vertically polarized.

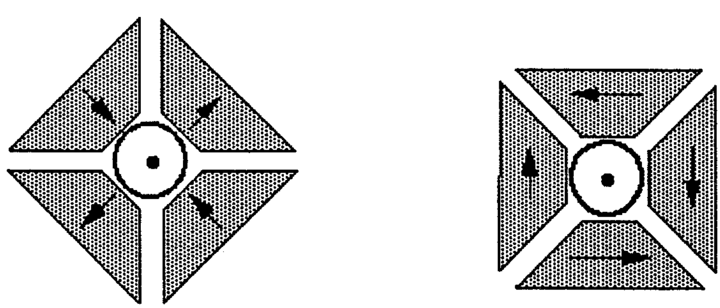

Figure 8.1-2. Cross-sectional views of Halbach (left) and Panofsky (right) pure permanent magnet quadrupole focusing corrector magnets. The arrows show the direction of magnetization in blocks of permanent magnet material.

condition and acts as a field clamp that reduces the fringe fields extending beyond the end of the structure to the right. Beyond the shunt plate to the right as shown also in **Fig. 8.2-7** are two magnetically detached shield plates which further reduce the fringe fields of the structure. Preliminary 3-D calculations show less than 10 G fields at 2 cm beyond the center of pole 0.

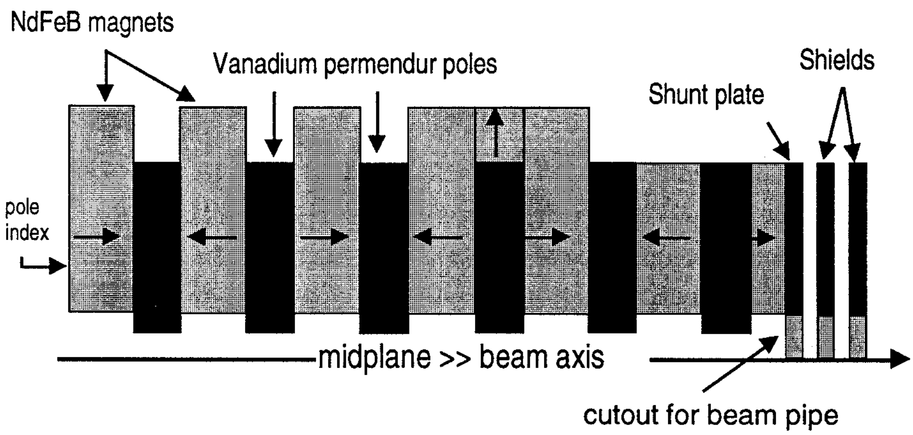

Figure 8.2-7. Cross-section of end structure with reduced P.M. material between poles 0 and 1 and increased material at pole 2.

The midplane field results are shown in the graph of **Fig. 8.2-8**. This graph includes the B_y field on the midplane of the device and the first and second integrals of the field, which give the beam steering and trajectories. This preliminary design shows: (1) good peak-to-peak uniformity leading up to the last pole of the device, and (2) small steering first integral and rapid termination of the fields beyond the steering pole. By adjusting the P.M. quantities in the structure, the net first integral can be brought arbitrarily close to zero to eliminate the end steering.

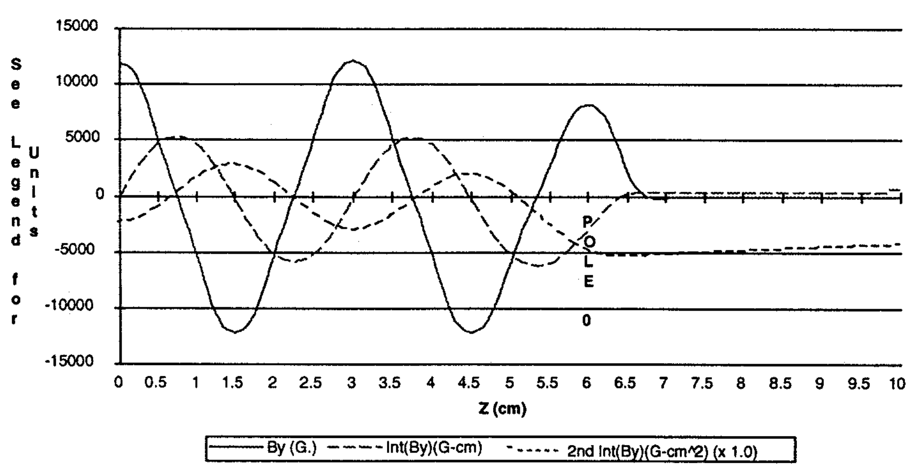

Figure 8.2-8. Graph of B_y with first and second integrals of B_y which give the steering field and normalized beam trajectory. The horizontal axis is z (cm).

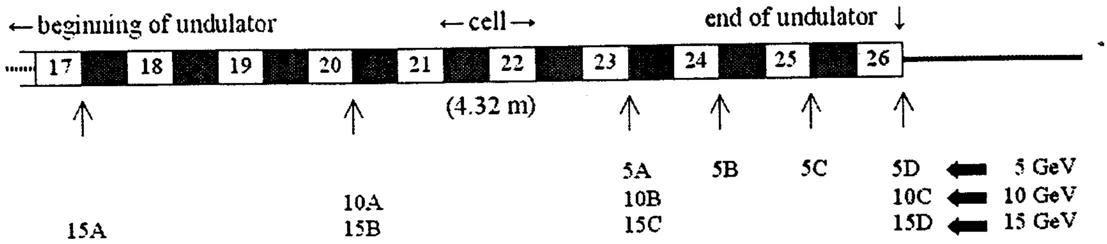

Figure 8.6-4. Proposed locations (up-arrows) of undulator wire scanners for optimal emittance measurement at 5-15 GeV. The last 9.5 cells of 26 in the undulator are shown. Wire groupings for the three energies are labeled A-C or A-D with an energy prefix of 5, 10 or 15 GeV.

Table 8.5-2. Beam-based undulator alignment procedure. Beam energy is 14.3 GeV unless otherwise noted.

Step #	Description	time/hr
0	Adjust the 2nd bunch compressor chicane for a ~150 μm electron bunch length to minimize transverse wakefields in the undulator	0.5
1	Adjust the launch using best position and angle fit to 1st 10 BPMs	0.1
2	Apply weighted steering to reduce (not zero) both the absolute BPM readings (÷50 μm) and the applied mover changes (÷50 μm)	0.2
3	Save ~100 sets of BPM readings for each of 5, 10, and 14.3 GeV beam energies while scaling upstream magnets to new energy each time	3
4	Run BPM data through analysis program to determine BPM and quadrupole offsets (select from data sets to minimize orbit jitter)	0.1
5	Adjust launch position and angle to remove determined linear component of BPM and quadrupole offsets	0.1
6	Set quadrupole movers to new positions and correct BPM offsets	0.1
7	Steer offset-corrected BPM readings to approximately zero using a minimum number of magnet movers	0.2
8	Repeat steps 3-7 until peak BPM readings at 4.5 GeV are <~50 μm	3.5/ iteration

- **summary**

  - **continuing development of strong-focusing technology**

    - **storage rings**

      - smaller, lower energy rings, longer smaller-gap undulators
      - stimulus for emittance, vacuum pressure reduction
      - limit (micropole undulators?)
      - alternative insertion device (ID) technologies (E&M ?)

    - **linac-driven XRFELs**

      - shorter FEL IDs